Diagnosing quantum transport from wave function snapshots

Devendra Singh Bhakuni,[1] Roberto Verdel,[1] Cristiano Muzzi,[2,3] Riccardo Andreoni,[1,2] Monika Aidelsburger,[4,5,6] and Marcello Dalmonte[1]

[1]*The Abdus Salam International Centre for Theoretical Physics (ICTP), Strada Costiera 11, 34151 Trieste, Italy*
[2]*SISSA – International School of Advanced Studies, via Bonomea 265, 34136 Trieste, Italy*
[3]*INFN, Sezione di Trieste, via Valerio 2, 34127 Trieste, Italy*
[4]*Max-Planck-Institut für Quantenoptik, 85748 Garching, Germany*
[5]*Faculty of Physics, Ludwig-Maximilians-Universität München, Schellingstrasse 4, D-80799 Munich, Germany*
[6]*Munich Center for Quantum Science and Technology (MCQST), Schellingstrasse 4, D-80799 Munich, Germany*

(Received 24 July 2024; revised 1 October 2024; accepted 4 October 2024; published 21 October 2024)

We study nonequilibrium quantum dynamics of spin chains by employing principal component analysis on data sets of wave function snapshots and examine how information propagates within these data sets. The quantities we employ are derived from the spectrum of the sample second moment matrix, built directly from data sets. Our investigations on several interacting spin chains featuring distinct spin or energy transport reveal that the growth of data information spreading follows the same dynamical exponents as that of the underlying quantum transport of spin or energy. Specifically, our approach enables an easy, data-driven, and, importantly, interpretable diagnostic to track energy transport with a limited number of samples, which is usually challenging without any assumption on the Hamiltonian form. These observations are obtained at a modest finite-size and evolution time, which aligns with experimental and numerical constraints. Our framework directly applies to experimental quantum simulator data sets of dynamics in higher-dimensional systems, where classical simulation methods usually face significant limitations and apply equally to both near- and far-from-equilibrium quenches.

DOI: 10.1103/PhysRevB.110.144204

I. INTRODUCTION

Over the last decade, the application of data science methods to physical phenomena has witnessed a significant surge across diverse fields [1]. Within the realm of condensed matter and statistical physics, unsupervised and nonparametric learning techniques have been utilized to diagnose physical phenomena, such as identifying phase transitions and critical behavior [2–7], clarifying the complexity of the problem by extracting the relevant degree of freedom without relying on prior knowledge of an *order parameter*. While by now well established at equilibrium, the applicability of these techniques beyond that has just started to be explored [8–14]. Therefore, it becomes crucial to delve into the potential of such methods in more intricate nonequilibrium setups.

Unlike equilibrium systems, where information is encoded into partition functions, out-of-equilibrium systems [15–17] pose greater complexity and simultaneously exhibit a wealth of fundamental phenomena such as dynamical phases of matter [18–24], anomalous quantum transport, and universal dynamics [25–49]. Most importantly, such classes of phenomena are immediately accessible to quantum simulators and computers, where out-of-equilibrium dynamics are often easier to access than equilibrium. These settings are also particularly attractive from a data-science viewpoint, as experimenters are now capable of generating snapshots of the full many-body wave function via projective measurements [42,50–55]—which are, however, often analyzed by relying on specific local and few-body observables. This requires specific *a priori* knowledge of the underlying dynamics and discards an uncontrolled amount of—potentially critical—information. Given that such wave function snapshots encode extensive information about the entire many-body state, several questions arise: Can we uncover essential physics *solely* from such observations without presuming an order parameter? How does information propagate within this data, and how does it relate to dynamic phenomena such as quantum transport? And, importantly, can we achieve this with assumption-free and yet interpretable methods?

In this study, we address these questions by presenting a technique for extracting relevant physics from snapshots of wave functions during real-time dynamics. Utilizing principal component analysis (PCA) [56] on collections of these snapshots, we study the dynamics of information propagation within the data sets and their connection with the underlying quantum transport. The simplicity of PCA, which builds on the singular-value decomposition (SVD) [56], enhances interpretability: this enables a direct link between observations and underlying physical phenomena that we elucidate analytically for spin-1/2 systems. Intuitively, the PCA highlights the most significant degrees of freedom, thereby genuinely identifying transport carriers if present on the analyzed basis.

The first model we treat as a paradigm for spin transport is the one-dimensional XXZ chain where the spin hydrodynamics has been extensively studied both theoretically [36,57–75] and experimentally [42–45,76–78] (for other related models, see Refs. [53,79–81]). We observe that the Shannon entropy derived from the PCA spectrum (that we denote as PCA entropy) and the information transfer, defined as the difference between the largest PCA eigenvalue of the left and right data

sets, increase with the same dynamical exponent as the underlying spin transport. Specifically, in the easy-plane case, we observe a linear growth of PCA entropy and the information transfer, whereas in the isotropic and easy-axis cases, we observe sublinear growth with distinct dynamical exponents consistent with the transport exponent. Furthermore, we establish an analytical link between the information transfer and the polarization transfer used in experiments to probe the nature of spin transport [42].

For energy transport, we study various quantum spin chains such as Ising [82], XYZ [83], and PXP models [84], where energy is the sole conserved quantity, resulting in diffusive, ballistic, and superdiffusive energy transport, respectively. Remarkably, we observe that the PCA entropy always grows with the same dynamical exponent as the energy transport, even at timescales where the conventional measure, i.e., the energy transfer, does not yet describe the correct universality class. These observations establish a link between information spreading within the datasets and energy transport dynamics. Our analysis offers an alternative, practical approach to investigate energy transport—a task typically challenging to achieve experimentally, in the absence of major assumptions on the Hamiltonian form.

Lastly, we incorporate random spin-flip imperfections into the data sets, often stemming from measurement errors in experiments. PCA entropy remains robust against such imperfections, accurately predicting the correct dynamical spin or energy exponent even with a moderate amount of spin-flip errors. This resilience underscores the reliability and applicability of PCA in analyzing quantum transport phenomena in realistic experimental conditions.

The paper is organized as follows. We provide a general workflow and define the quantities of interest in Sec. II, followed by the applicability of the method for spin transport in Sec. III and energy transport in Sec. IV. In Sec. V, we discuss the effect of imperfect measurements. Finally, we summarize our findings in Sec. VI.

II. GENERAL WORKFLOW: DATA PIPELINE

The workflow outlined in this study comprises three primary steps: (i) dynamical evolution and wave function sampling, (ii) data analysis based on PCA, and (iii) extraction of the relevant physics (Fig. 1).

(i) *Dynamical protocol and sampling.* The first step involves evolving a quantum many-body state under a given Hamiltonian H that describes an interacting quantum lattice model defined on L sites, with some global conserved quantity $\mathcal{Q}$. In our protocol, we imprint an imbalance of the conserved quantity $\mathcal{Q}$ in the initial state, a standard approach in transport studies [42,59,85]. For simplicity, in the following we only consider spin-1/2 (qubit) systems, although our approach can be extended to systems with a larger local Hilbert-space dimension [86].

The system dynamics are probed at selected evolution times via projective measurements on a given basis with single-site resolution. The outcome of such measurements are bit strings $\mathbf{n} = (n_1, \ldots, n_L)$, with $n_j \in \{0, 1\}$ for $j = 1, \ldots, L$, which are dubbed *wave function snapshots* [87]. For each evolution time, the sampled wave function snapshots

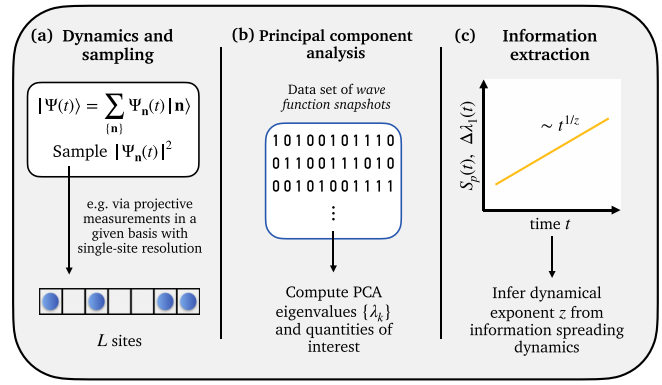

FIG. 1. Schematic of our data-driven framework for diagnosing quantum transport. (a) We consider quantum many-body dynamics with an initial imbalance in a global conserved quantity $\mathcal{Q}$. At each evolution time t, the many-body wave function is sampled, e.g., via projective measurements in a given basis. (b) Data sets of the sampled *wave function snapshots* are then subject to a principal component analysis. (c) The dynamics of PCA spectral quantities, such as the entropy S_p and the largest eigenvalue λ_1—quantifying information propagation—are governed by the relevant dynamical exponent, allowing us to diagnose the nature of transport without prior knowledge of an order parameter.

are organized as the row vectors of a rectangular data matrix, $\mathbf{X}(t) = \{\mathbf{n}^{(i)}(t)\}$, where $i = 1, \ldots, N_r$ labels different realizations. Importantly, specific knowledge of the Hamiltonian H is, in fact, not needed as long as we have access to the relevant wave function snapshots.

(ii) *Data analysis by principal components.* Each data matrix $\mathbf{X}$ (to simplify the notation below, we omit the explicit time dependence unless needed) is then analyzed within the mathematical framework of PCA. We perform an eigenvalue decomposition of an $L \times L$, symmetric matrix

$$\mathbf{\Sigma} = \frac{1}{N_r}\mathbf{X}^T\mathbf{X}. \tag{1}$$

We sort the eigenvalues of this matrix in nonincreasing order, $\lambda_1 \geqslant \cdots \geqslant \lambda_R > 0$, where R is the rank of both $\mathbf{\Sigma}$ and $\mathbf{X}$. In practice, this is conveniently done via a SVD of $\mathbf{X}$, with λ_k determined from the corresponding singular value s_k of $\mathbf{X}$, through $\lambda_k = \frac{1}{N_r}s_k^2$. The quantities of interest are then defined from the set of eigenvalues, $\{\lambda_k\}$. We note that the PCA algorithm above differs from its standard version [56] in that no centering of the data (removing the sample mean of each column from its entries) is performed. While this implies that the result of our analysis is sensitive to the choice of classical encoding of the observations $\{\mathbf{n}^{(i)}\}$, as discussed later on, the results presented below are, in general, robust for sensible choices of such encoding.

Throughout our work, we primarily concentrate on the *PCA entropy* [11,88,89], which is a Shannon entropy defined on the normalized spectrum of $\mathbf{\Sigma}$, namely,

$$S_p = -\sum_{k=1}^{R} \bar{\lambda}_k \ln(\bar{\lambda}_k), \tag{2}$$

where $\bar{\lambda}_k = \lambda_k / \sum_l \lambda_l$. Note that the set $\{\bar{\lambda}_k\}$ formally defines a probability distribution as $\bar{\lambda}_k$ are non-negative and sum to one. Additionally, we examine the behavior of the largest eigenvalue λ_1, which measures the *variability* (i.e., statistical information) of the data along the first "principal direction," which is determined by the corresponding eigenvector $\vec{v}_1$. Both of these metrics, in their respective ways, quantify the spread of information within the wave function data sets.

(iii) *Information extraction.* Finally, physically relevant information, such as dynamical exponents, is extracted from the temporal scaling of these quantities. Given that PCA identifies the most pertinent degree of freedom to characterize the data, the question arises whether transport, in terms of data, can be considered "simple." If so, the analysis based on PCA should yield the correct transport exponents corresponding to the conserved quantity $\mathcal{Q}$. We hypothesize that this is the case due to conserved quantities dominating the constraints in the data set, implying that both PCA entropy and the largest eigenvalue λ_1 will provide valuable insights. The remainder of the paper will scrutinize our conjecture for spin and energy transport in various quantum spin models, and provide analytical arguments in support of that.

III. SPIN TRANSPORT

We first demonstrate the application of the above methodology to study spin transport. We consider the one-dimensional (1D) XXZ chain of L sites as a prototypical model, with the Hamiltonian given by

$$H = \sum_i \left(S_i^x S_{i+1}^x + S_i^y S_{i+1}^y\right) + J_z \sum_i S_i^z S_{i+1}^z. \tag{3}$$

Here, $S_i^k, k = x, y, z$ are spin-1/2 operators at site i, J is the strength of the interaction in the XY plane, which we set to $J = 1$ in all our numerical simulations, and J_z is the anisotropy parameter. This model conserves the total magnetization along the z axis, i.e., $[H, \sum_i S_i^z] = 0$, and thus allows the study of spin transport [36,42,57–76].

The behavior of spin transport and universality classes can be obtained by focusing on the infinite-temperature correlation functions [29,30,36,60,84] or by studying the dynamics of starting from an initial inhomogeneous state having opposite magnetization in the two halves of the chain [59,85]. Such an initial state can be written as

$$\rho(0) \sim (1 + \eta\sigma^z)^{\otimes L/2} \otimes (1 - \eta\sigma^z)^{\otimes L/2}, \tag{4}$$

where the parameter η controls the magnetization of the chain with the two halves corresponding to the magnetization $\pm\eta/2$. In the limit of $\eta = 1$, the initial state reduces to a perfect domain-wall state.

The nature of the transport is then characterized by looking at the polarization transfer between the two halves and is defined as [42,60]

$$\Delta P(t) = 2\,[P^L(t) - P^R(t)]. \tag{5}$$

Here, $P^{L/R}$ is the total magnetization variation over time of the left and right half of the chain, respectively, and is given by

$$P^{L/R}(t) = \sum_{i \in L/R} \left[\left\langle S_i^z(t)\right\rangle - \left\langle S_i^z(0)\right\rangle\right]/2. \tag{6}$$

The polarization transfer grows as a power law $\Delta P(t) \sim t^{1/z}$, with z being the dynamical exponent, distinguishing the different transport regimes. For the 1D XXZ model, at the isotropic point $J_z = 1$, the infinite-temperature transport is known to be superdiffusive, with a dynamical exponent $z = 3/2$ corresponding to the Kardar-Parisi-Zhang (KPZ) universality class [42,59,60]. On the contrary, for the easy-plane ($J_z < 1$) and easy-axis ($J_z > 1$) regimes, the transport is ballistic and diffusive, respectively [90], with the dynamical exponent being $z = 1$ and $z = 2$, respectively. It is worth mentioning that for the pure domain wall $\eta = 1$ and at the isotropic point $J_z = 1$, the dynamics cross over to diffusion at long times [91,92]. However, in the experimentally accessible times, the dynamics remain superdiffusive [42]. Similarly, for $J_z \gg J$, the dynamics from a domain-wall initial state are also frozen. Here we will focus on values of $J_z \gtrsim J$, for which the polarization transfer exhibits transient dynamics.

In the following, we focus on both the pure domain-wall initial state and the partially polarized domain-wall initial state. To simulate the system dynamics, we employ the time-evolving block decimation (TEBD) method [93,94] for a system size up to $L = 150$ and with a truncation error of 10^{-8}. We built the data matrix by a perfect sampling [95,96] of a matrix product state (MPS) representation of the time-evolved state at different times, starting from a given initial state. The perfect sampling algorithm works via systematic evaluations of the conditional probability distribution in an MPS. It computational cost scales as $Ld\chi^3$, where χ is the bond dimension, L is the length of the chain, and d is the physical dimension (here, $d = 2$). Thus, for a reasonable value of χ, one can still *efficiently* sample a MPS-based probability distribution, even for $L \sim O(10^2)$. Of course, for such system sizes, we can only sample, in a practical manner, a number of snapshots, $N_r \ll d^L$. Crucially, this is exactly the regime in which our method has been devised to work.

A. Pure domain-wall dynamics

We first consider the case of a pure domain-wall initial state [$\eta = 1$ in Eq. (4)] and study the dynamics of the information propagation at the data set level.

PCA entropy. We plot the dynamics of the PCA entropy $S_p(t)$ in Fig. 2(a) for various interaction strengths $J_z = 0.5,\ 1.0,\ 1.1$, corresponding to ballistic, superdiffusive, and diffusive transport for $N_r = 2000$ samples per evolution time. As a key observation, we find that the PCA entropy grows as a power law in time $S_p \sim t^{1/z_s}$, and captures the correct dynamical exponents $z_s \approx z$, for all three cases. Dashed lines in this figure show the power-law growth with the dynamical exponent z.

To investigate the dependence on the number of samples, we fix the interaction strength $J_z = 1$ and plot in Fig. 2(b) the dynamics of S_p for various values of $N_r = 100$–2000. We see that even for a small number of samples, $N_r \sim 100$, S_p shows a power-law growth with the dynamical exponent z_s close to 3/2.

A more systematic analysis of the dynamical exponent $\beta_s = 1/z_s$ extracted from the PCA entropy is plotted in Fig. 2(e) as a function of N_r and for a range of system sizes, $L = 50$–150. For larger system size and number of samples,

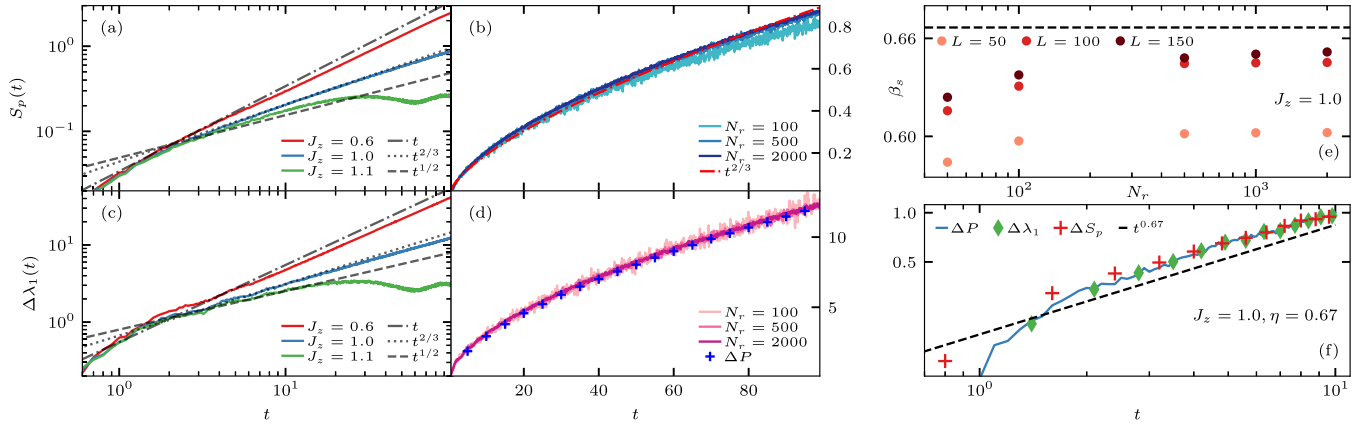

FIG. 2. Spin transport: (a)–(d) Dynamics of the PCA entropy S_p and information transfer $\Delta\lambda_1(t)$ for different parameters starting from a domain wall for $L = 150$ and $J = 1$. (a),(c) S_p and $\Delta\lambda_1(t)$ on varying the interaction strength J_z at fixed $N_r = 2000$. (b),(d) S_p and $\Delta\lambda_1(t)$ on varying the number of samples, N_r, at fixed $J_z = 1.0$. The blue markers in (d) correspond to the polarization transfer. (e) The dynamical exponent β_s as a function of N_r extracted from $S_p(t)$ for $J_z = 1.0$. (f) The dynamics of *normalized* polarization transfer ΔP, information transfer $\Delta\lambda_1$, (t), and entropy transfer $\Delta S_p(t)$ starting from an infinite-temperature state ($\eta = 0.67$). The dashed/dotted lines provide a guide to different transport regimes.

the exponent approaches the correct dynamical exponent $\beta = 1/z$ (marked by the dashed line). Moreover, even for a small number of samples ($N_r = 100$), the exponent is also quite close to the dynamical exponent z, suggesting that a limited number of samples is enough to obtain the information about the underlying transport. We note that even the larger volumes are still a few percent off the expected decay: such accuracy has to be expected, as we are utilizing data over timescales of the order of 100 J^{-1}, which, likely, limits our accuracy at the percent level. Additionally, the other source of this departure from the KPZ dynamical exponent could be because the superdiffusive behavior crosses over to diffusion at a late time for the domain-wall initial state [91,92]. We do not observe a clear scaling with N_r, but we expect, at least for larger system sizes, a systematic improvement scaling as $\sqrt{N_r}$.

Information transfer via largest PCA eigenvalue. So far, we have analyzed information from the entire wave function. We now scrutinize how information propagates between the two halves of the data set. For this purpose, we concentrate on the largest eigenvalue $\lambda_1(t)$ of the matrix of second moments $\mathbf{\Sigma}$ in Eq. (1). Motivated by the experimentally relevant observable $\Delta P(t)$, we define the *information transfer* as

$$\Delta\lambda_1(t) = 2\big[\Lambda_1^L(t) - \Lambda_1^R(t)\big], \tag{7}$$

where $\Lambda_1^{L/R}(t) := -[\lambda_1^{L/R}(t) - \lambda_1^{L/R}(0)]/2$. Here, we first divide the data set into left and right data subsets that are comprised of a $N_r \times L/2$ matrix each, and compute $\lambda_1^{L/R}(t)$ of the left/right data subset separately. We *purposely* focus on single eigenvalues to test the conjecture: Is spin transport a simple phenomenon (that is, something that can be accurately captured by a minimal number of variables in the context of wave function snapshots) or is it not?

In Fig. 2(c), we plot the dynamics of $\Delta\lambda_1(t)$ as a function of time for $L = 150$ and various values of the interaction strength J_z. Similar to the PCA entropy, the information transfer between the two data subsets happens with the same growth exponent z. The dependence of the information transfer on the number of samples is provided in Fig. 2(d) for $J_z = 1.0$. This plot also shows the dynamics of the polarization transfer $\Delta P(t)$ computed from our TEBD simulations (shown by blue cross markers). Interestingly, we find that the information transfer $\Delta\lambda_1(t)$ not only provides the correct dynamical exponents for a small number of samples, but also approximates the polarization transfer $\Delta P(t)$ quite well.

B. Relationship between information transfer and transport

The agreement between the information transfer and the polarization transfer can be understood using a fundamental theorem on SVD, which states that for any matrix $\mathbf{A}$, the sum of its squared singular values equals the square of its Frobenius norm, i.e., $\sum s_k^2(\mathbf{A}) = ||\mathbf{A}||_F^2 = \sum_{i,j} \mathbf{A}_{i,j}^2$ [97]. Since the entries of the data matrices considered here are 0 or 1, the previous result implies that

$$\sum_{k=1}^{R} s_k^2(\mathbf{X}) = \sum_{i,j} n_j^{(i)} = N_r\left(\frac{L}{2} - S\right), \tag{8}$$

where $S = \frac{1}{N_r}\sum_{i=1}^{N_r}\sum_{j=1}^{L}\frac{1}{2}s_j^{(i)}$, with $s_j \in \{-1, 1\}$, is the average total magnetization estimated from the snapshots. Thus, applying this result to the left and right data subsets mentioned above and the fact that $\lambda_k = s_k^2/N_r$, we obtain

$$\lambda_1^{L/R}(t) = [L/2 - S^{L/R}(t)] - \sum_{k>1}\lambda_k^{L/R}(t). \tag{9}$$

In our numerical calculations, we observe that $\sum_{k>1}\lambda_k^L(t) \approx \sum_{k>1}\lambda_k^R(t)$ for all accessed times. Hence, when considering the difference $\lambda_1^L(t) - \lambda_1^R(t)$, such terms cancel each other out and we get

$$\Delta\lambda_1(t) \approx \Delta P(t), \tag{10}$$

with the definitions in Eqs. (5) and (7). We have also numerically verified this relationship for the case of ballistic and diffusive transport, respectively.

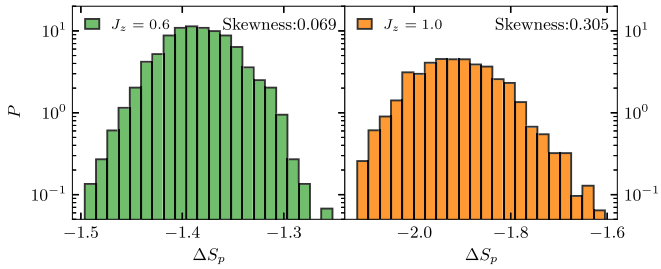

FIG. 3. Probability distribution of the entropy transfer ΔS_p between the left and right data sets. Left: For ballistic transport ($J_z = 0.6$), the distribution becomes symmetric with skewness 0.069. Right: For KPZ superdiffusive transport ($J_z = 1.0$), the distribution becomes asymmetric with skewness 0.305.

Distribution of information and entropy transfer

The above relationship also implies that the distribution of the information transfer for batches of the data set can feature the Tracy-Widom distribution, a hallmark of the KPZ universality class [42]. Interestingly, not only the information transfer but, in fact, the whole *entropy transfer* between the two halves of the system, which considers *all* eigenvalues and is defined as

$$\Delta S_p(t) = S_p^L(t) - S_p^R(t), \tag{11}$$

where $S_p^{L/R}$ is the PCA entropy of the left and right data sets, respectively, follows the Tracy-Widom distribution. We compare the distribution of the entropy transfer for the ballistic ($J_z = 0.6$) and the KPZ ($J_z = 1.0$) cases in Fig. 3. For ballistic transport, the distribution of the entropy transfer becomes symmetric, while for $J_z = 1$, we see the emergence of the Tracy-Widom distribution, which confirms the KPZ superdiffusive transport at $J_z = 1$.

C. Infinite-temperature spin transport

In this section, we consider the infinite-temperature inhomogeneous state defined in Eq. (4) with $\eta = 0.67$. The evolution of the mixed-density matrix is, however, challenging for larger system sizes. Instead, here, for numerical purposes, we start with ensembles of random product states given by

$$|\Psi(0)\rangle = \bigotimes_{i<L/2} |\psi(+\eta, \phi_i)\rangle \bigotimes_{i\geqslant L/2} |\psi(-\eta, \phi_i)\rangle, \tag{12}$$

with $|\psi(-\eta, \phi_i)\rangle = \sqrt{(1+\eta)/2}|\uparrow\rangle + e^{i\phi_i}\sqrt{(1-\eta)/2}|\downarrow\rangle$, and ϕ_i are drawn randomly from the uniform distribution $\phi_i \in [0, 2\pi)$. Averaging over the ensemble of these pure states is equivalent to an infinite-temperature density matrix in Eq. (4) [59].

We consider $M = 40$ random product states and generate N_r configurations for each ϕ_i. We build a new data matrix of size $(MN_r) \times L$ to perform the PCA. Due to the nature of the initial high-energy state, the PCA entropy $S_p(t)$ of the full data set saturates rather quickly and is unsuitable for characterizing spin transport. We, therefore, rely on the information transfer between the left and right data sets. Additionally, we also study the entropy transfer between the two halves of the chain introduced in Eq. (11).

In Fig. 2(f), we plot the dynamics of the normalized polarization transfer, the normalized entropy difference, and the normalized information transfer for $L = 100$ and at a fixed interaction strength $J_z = 1.0$. Similar to the domain-wall initial state, we see that the dynamics of these quantities grow as a power law, which is close to the KPZ dynamical exponent (shown as the dashed line) and thus highlights the applicability of our analysis for a broader class of initial states.

D. Summary: Spin transport from data sets

In summary, by performing PCA on the data sets representing the wave function snapshots, we found that the quantities such as PCA entropy and information/entropy transfer grow with the same dynamical exponent as the underlying spin transport. We show this for two different choices of initial states, namely, the perfect domain-wall initial state and an inhomogeneous infinite-temperature state. Additionally, we provide an analytical understanding of the observed features of the information transfer, which can be approximated to the polarization transfer.

Since the largest eigenvalue of the PCA spectrum is enough to extract the dynamical exponent of spin transport, this implies that spin transport is a fundamentally simple phenomenon at the data level and can be inferred by dimensionality reduction.

IV. ENERGY TRANSPORT

We now investigate energy transport, focusing specifically on systems with energy being the only conserved quantity and systems where energy conservation is accompanied by magnetization conservation. In general, akin to spin transport, the characteristics of energy transport can be elucidated by analyzing infinite-temperature *energy-energy* correlation functions [82,85]. However, unlike spin transport, which has been experimentally observed, probing energy transport poses significant challenges in experiments. It requires the precise form of the local energy function, which is heavily reliant on assumptions, and generically requires measurement on all possible bases, as well as interbasis measurements.

Following the choice of the initial state for the spin transport, we consider the initial state with an *energy domain wall* [85] by preparing the left half in the ground state of Hamiltonian $+H$ and the right half in the ground state of the Hamiltonian $-H$, respectively [98]. At $t = 0$, the two halves of the chains are joined and the system evolves according to the full Hamiltonian H. We do not make any assumption on what the specific form of the Hamiltonian is.

The nature of the energy transport can be characterized by focusing on the energy transfer between the two halves, defined as

$$\Delta E(t) = E_L(t) - E_R(t), \tag{13}$$

where $E_{L/R}(t) = \sum_{i\in L/R}[\langle H_i(t)\rangle - \langle H_i(0)\rangle]/2$ is the total energy of the left and the right parts, respectively. Starting from the aforementioned initial state, the energy transfer grows as a power law $\Delta E \sim t^{1/z_\epsilon}$, where the dynamical exponent z_ϵ provides information about the nature of the transport. A dynamical exponent of $z_\epsilon = 1$ signifies ballistic transport,

whereas $z_\epsilon = 2$ characterizes diffusion. When $z_\epsilon < 2$, energy propagation exhibits superdiffusive behavior, whereas $z_\epsilon > 2$ indicates subdiffusive energy transport.

To perform PCA, similar to the previous scenario, we construct the data matrix by collecting the snapshots on the σ^z basis at different times. Notably, in the examined model, measurements in the σ^z basis suffice to discern the hallmark of the underlying energy transport. This is one of the key observations presented in this work. A detailed exploration of alternative basis choices will be presented elsewhere.

In the following, we consider different quantum many-body systems featuring distinct energy transport.

A. Energy-conserving models

We first consider systems where energy is the only conserved quantity and focus on models that exhibit different types of energy transport.

1. Ising model

We consider a nonintegrable one-dimensional mixed-field Ising model (MFIM), with the Hamiltonian

$$H = g\sum_{i=1}^{L}\sigma_i^x + \sum_{i=2}^{L-1} h\sigma_i^z + (h-J)\left(\sigma_1^z + \sigma_L^z\right) + J\sum_{i=1}^{L-1}\sigma_i^z\sigma_{i+1}^z. \tag{14}$$

Here, g and h correspond to the strength of the transverse and the longitudinal field, respectively, and J is the strength of interaction along the z direction. For our numerical simulations, we fix the parameters $J = 1$, $g = (\sqrt{5}+5)/8$, and $h = (\sqrt{5}+1)/4$. In this nonintegrable model, it is established that the entanglement entropy grows ballistically in time, while the energy spreading is diffusive ($\Delta E \sim t^{1/2}$) [82].

2. XYZ model

In addition, we investigate a system wherein energy transport follows a nondiffusive behavior. To this end, we concentrate on an integrable one-dimensional XYZ spin chain, where energy transport is recognized to be ballistic [83]. The model Hamiltonian can be written as

$$H = \sum_i J_x\sigma_i^x\sigma_{i+1}^x + J_y\sigma_i^y\sigma_{i+1}^y + J_z\sigma_i^z\sigma_{i+1}^z, \tag{15}$$

where $J_x = J+\delta$, $J_y = J-\delta$, and J_z are the interactions along three directions and δ is the anisotropy parameter. We set $J_z, J = 1$, and $\delta = 0.1$ for numerical purposes.

3. Kinetically constraint PXP model

Finally, we consider a model where energy transport is neither ballistic nor diffusive, but the infinite-temperature energy transport is known to be superdiffusive. We consider a kinetically constrained PXP model [84,99], with the Hamiltonian given by

$$H = \Omega\sum_i P_{i-1}X_iP_{i+1}. \tag{16}$$

Here, X_i is the Pauli X matrix and Ω is the Rabi frequency, which we set to $\Omega = 1$. The operators $P_i = \frac{1-n_i}{2}$ are the local projectors on $|\downarrow\rangle$ state and discard the possibility of two up-spins being next to each other.

4. Numerical results

For the models discussed above, we perform the PCA on the generated data sets using exact diagonalization. Due to the choice of initial state (constructed from the ground state of subsystem Hamiltonians $\pm H$), we always have a nonzero initial value of the PCA entropy. Hence, in order to filter out this entropic contribution, we focus on the dynamics of the PCA entropy difference, $\tilde{S}_p(t) = S_p(t) - S_p(0)$.

We show the dynamics of $\tilde{S}_p(t)$ for various numbers of samples in Fig. 4, alongside the energy transport $\Delta E(t)$ [Eq. (13)]. For both the MFIM and XYZ chains, we verify that the energy transfer grows as a power law with the dynamical exponent being $z_\epsilon = 2$ and $z_\epsilon = 1$ [Figs. 4(d) and 4(e)], corresponding to the diffusive and ballistic transport, respectively. Interestingly, similar to the energy transport, the PCA entropy difference $\tilde{S}_p(t)$ also grows as a power law, $\sim t^{1/z_s}$ [Figs. 4(a) and 4(b)], capturing the correct dynamical exponent $z_s \approx z_\epsilon$. While for small values of $N_r = 1000$ we observe large fluctuations, increasing the number of samples (yet with $N_r \ll 2^L$) reduces the fluctuations significantly. Furthermore, we observe that the saturation of the PCA entropy and energy transfer happens at different timescales. The information spreading on the data set with snapshots only in the σ^z basis happens faster than the energy transfer. Such difference is likely due to finite volume effects acting differently on these quantities and not to the reduced statistics of PCA entropies (changing N_r has little effect on the saturation point).

Similarly, for the PXP model, we illustrate the dynamics of the PCA entropy difference and the energy transfer ΔE in Figs. 4(c) and 4(f). The energy transfer grows as a power law with dynamical exponent $1/z_\epsilon \approx 2/3$ (the discrepancy from the power law of $2/3$ is due to a finite-size effect; see, e.g., Ref. [84], which employ MPS simulations for larger system sizes). Similar to the energy transfer, the PCA entropy difference also grows with the same dynamical exponent. Thus, an analysis based on PCA can aid in determining the accurate dynamical exponent of energy transport and, in fact, can result as far superior to energy transfer: timescales of the order of 10, sample batches of the order of a few thousands, and sizes of the order of 30 sites are sufficient to correctly determine a dynamical scaling exponent. All of these are well attainable in Rydberg quantum simulators [55].

B. Energy and spin conservation

So far, in this section, our focus has been on systems where energy is the sole conserved quantity. Now, we aim to assess the applicability of our analysis in predicting the nature of transport in systems that conserve both energy and magnetization. To this end, we turn our attention to the 1D XYZ chain with $\delta = 0$ and a fixed magnetization $\langle S^z\rangle = 0$. While spin transport exhibits superdiffusive behavior, energy transport is known to be ballistic in such systems. We examine the initial state featuring an energy domain wall, but with a homogeneous magnetization profile [see inset in Fig. 5(a)].

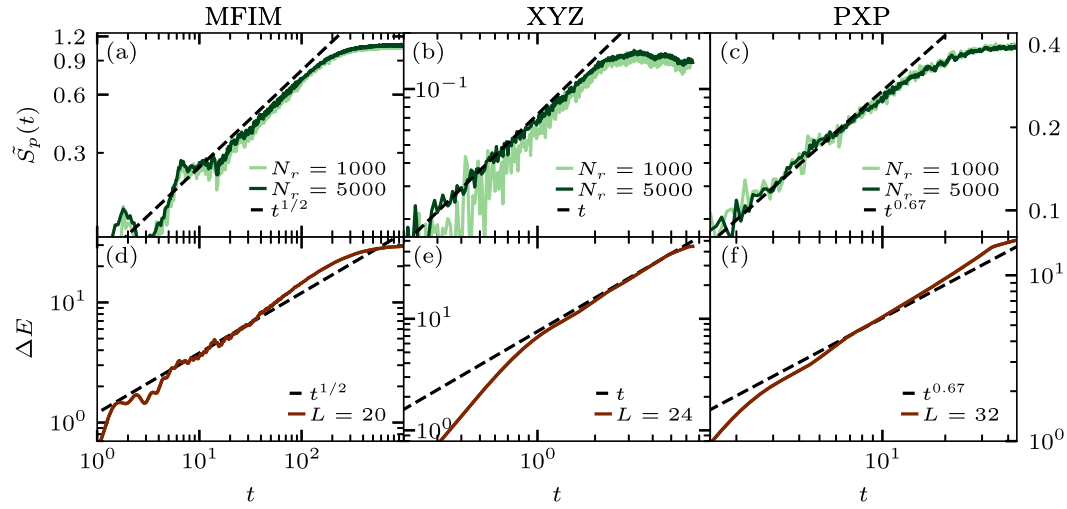

FIG. 4. Energy transport: Dynamics of PCA entropy $S_p(t)$ and the energy transport ΔE starting from an initial *energy domain-wall* state. (a),(d) For the MFIM, (b),(e) for the XYZ spin chain, and (c),(f) for the PXP model. The dashed lines provide a guide to the different transport regimes.

We plot the dynamics of the PCA entropy difference $\tilde{S}_p(t)$ for different numbers of samples, N_r, and the energy transfer ΔE in Figs. 5(a) and 5(b), respectively. We observe that the growth of both quantities follows a linear trend over time, indicating a ballistic nature of energy transport. Interestingly, the saturation time for information propagation on the data sets is relatively short compared to the energy transport. Thus, our analysis implies that by introducing a suitable kink in the density profile of the conserved quantity $\mathcal{Q}$ in the initial state, the analysis carried out here can effectively characterize the underlying transport of that conserved quantity $\mathcal{Q}$.

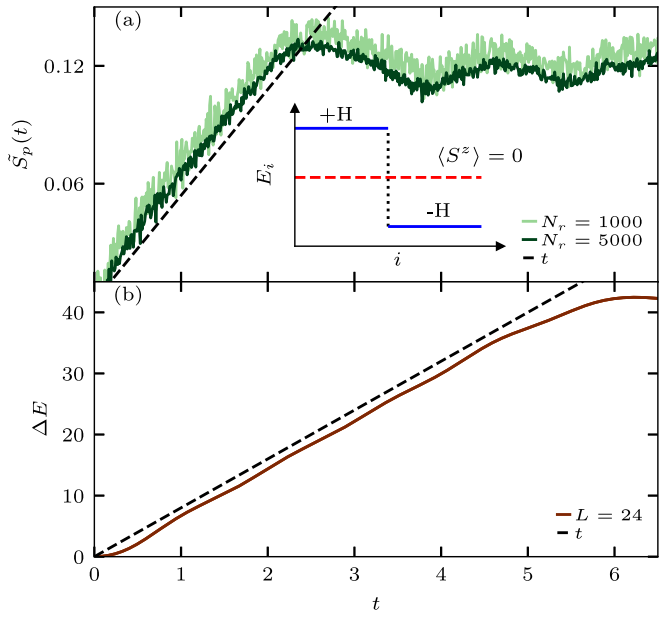

FIG. 5. Energy transport: Dynamics of PCA entropy $S_p(t)$ and the energy transport ΔE in the XXZ model, starting from an initial *energy domain-wall* state, but with a conserved homogeneous magnetization profile, as schematically shown in the inset in (a).

C. Summary: Energy transport from data sets

To summarize, in this section, we demonstrate the utility of PCA for characterizing energy transport in various setups, conserving only total energy or both total energy and magnetization, each with a distinct nature of energy transport. Our analysis suggests that the information about the underlying energy transport can be extracted from PCA entropy, which grows with the same dynamical exponent. In analogy to spin transport, similar results can be obtained using the largest eigenvalue, albeit with larger errors.

It is noteworthy to highlight that while spin transport has been investigated in experiments, observing energy transport presents a significant challenge. However, our findings indicate that energy transport can be deduced from wave function snapshots on the z basis, a data type readily accessible in experiments that offers a promising avenue for studying energy transport in experiments. And, importantly, short times and small volumes already indicate the correct dynamical exponent, in some cases with superior accuracy with respect to the (experimentally hard to access) energy transport measures.

V. EFFECT OF MEASUREMENT ERRORS AND ENCODING

A. Resilience against spin-flip measurement errors

In this section, we consider the effect of imperfect measurements, which typically arise in realistic experimental settings and correspond to random spin slips. In the following, we show the robustness of our method in identifying the correct transport exponent, even with these imperfect measurements.

To this end, we introduce finite spin flips on our data set at each time instance. On the data level, this amounts to changing the bit value (“0” to “1” and vice versa) on a fraction of sites q that is chosen randomly for each snapshot. Such a flipping process introduces an extra contribution to the PCA entropy in the initial state. Therefore, we focus on the PCA entropy difference $\tilde{S}_p(t)$ previously introduced [Eq. (11)]. To illustrate

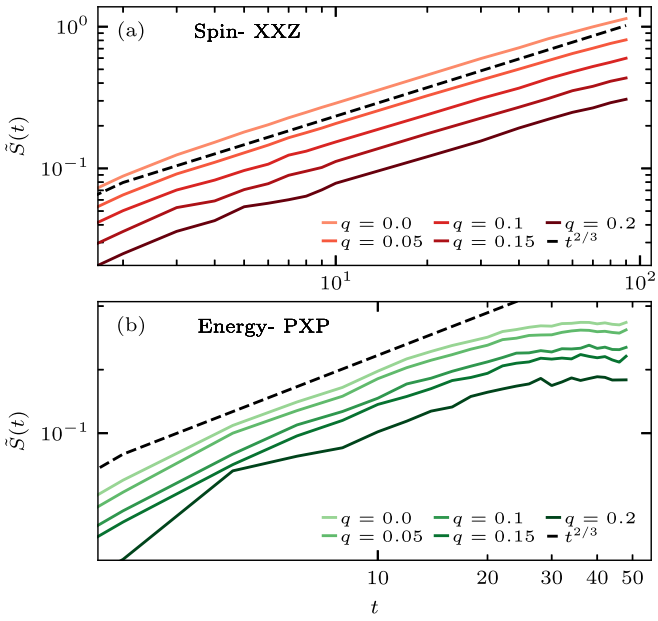

FIG. 6. Finite measurement errors: Dynamics of the PCA entropy difference $\tilde{S}_p(t)$ for imperfect measurement with spin-flip fraction q, for (a) spin transport in the XXZ model and (b) energy transport in the PXP model. The dashed black line provides a guide to the power law $t^{2/3}$.

this, we specifically focus on the spin transport in the XXZ model and the energy transport in the PXP model. We have checked that similar results hold for the energy transport in the MFIM and XYZ models.

Figure 6 depicts the dynamics of the PCA entropy difference $\tilde{S}_p(t)$ for the spin transport in the XXZ model [Fig. 6(a)] and for the energy transport in the PXP model [Fig. 6(b)] for various flipping fraction q and with a fixed number of samples, $N_r = 5000$. The dynamical exponent corresponding to the spin transport in the XXZ model and the energy transport in the PXP model predicts superdiffusion with $z, z_\epsilon \approx 3/2$. For both cases, $\tilde{S}_p(t)$ continues to grow as a power law even for a finite flipping fraction q. Notably, despite random flips for the selected probabilities, the dynamical exponents remain very close to $z, z_\epsilon \approx 3/2$. A guide to the power law $t^{2/3}$ is provided in Fig. 6 by a black dashed line, affirming the robustness of the PCA method in characterizing the dynamical exponent despite very considerable imperfections.

While we do not know the origin of the unexpected resilience of the protocol to measurement errors, it is worth emphasizing that at the information theoretical level, principal component spectra are known to undergo "learning" transitions in specific random matrix models [100]. It would be interesting to understand whether those transitions are related to the present observations and if they can provide additional knobs to control errors in case of other experimental imperfections.

B. Relevance of the encoding

The results mentioned above were obtained using an uncentered version of PCA. As noted before, this makes our analysis sensitive to the choice for representing the classical data $\mathbf{n} = (n_1, \ldots, n_L)$. Even when considering only an encoding with $n_j \in \{0, 1\}$, different numerical results are obtained upon "reversing" our convention, i.e., $n_j \to \tilde{n}_j = (n_j + 1) \bmod 2$. We found, however, that unless the data matrix is highly "homogeneous" [i.e., containing an overwhelmingly larger number of 0's (1's) than 1's (0's)], the dynamical exponents governing the growth of information spreading in both cases are consistent with each other. As an empirical observation, we found better results (smaller fluctuations in the information-spreading signal) in the representation for which the data points do not concentrate very close to the origin.

We note that with standard PCA, i.e., centering the data before performing an SVD on the data matrix $\mathbf{X}$, we were not able to extract information about the dynamical exponents associated with quantum transport, at least in the setting considered in this work. This becomes particularly clear when considering the information transfer in the XXZ model, whose relation to the polarization transfer noted in Sec. III B breaks down upon centering the data. We do not disregard, however, the potential usefulness of PCA with mean centering in different scenarios where statistics around the mean play a central role, as in the case of fluctuating hydrodynamics [54]. Here, on the other hand, it appears that the centroid of the data cloud itself reveals important physical information, and thus, uncentered PCA does provide informative insights.

VI. DISCUSSION AND OUTLOOK

Utilizing PCA on data sets of snapshots (in the z basis) of the full many-body wave function, we demonstrate that fundamental quantities derived from the singular values of the data matrix provide knowledge about the information spreading on the data set and its connection with the underlying nature of quantum transport of conserved quantities. This suggests that transport can be viewed as an emergent and relatively simple phenomenon from the perspective of information theory, accessible via linear dimensional reduction schemes. At the conceptual level, we conclude that data information transfer is dominated by conserved quantities, a highly nontrivial fact that for the spin-1/2 case, can be analytically connected to the specific structure of principal component analysis. Our findings are supported by numerical investigations across various interacting quantum spin chains exhibiting distinct energy or spin transport.

In terms of application to experiments, our method capitalizes on the capabilities of quantum simulators, leveraging wave function snapshots obtained through *in situ* and flexible basis imaging [42,50–55]. Importantly, our approach directly applies to experimental wave function snapshots of higher-dimensional quantum systems, where conventional numerical methods face limitations due to entanglement growth and exponential scaling of the Hilbert-space dimension. For the case of energy transport, we identify clear cases where the latter can be experimentally probed at a quantitative level, which is otherwise challenging if no input on the exact Hamiltonian functional is *a priori* given. Remarkably, for energy transport, we demonstrate that small volumes and reduced statistics are sufficient for accurately determining the dynamical exponents, suggesting that dimensional reduction is particularly effective for such dynamics—that is, energy

transport is simple at the data structure level. This may be particularly relevant to Rydberg atom quantum simulators [55], where our method predicts the correct universal properties already at small sizes, short evolution times, and at the price of modest statistics, in regimes where even energy transport measures are failing to get the correct physics.

Our work raises several intriguing questions for future exploration. For instance, it prompts investigation into whether these methods or their generalizations can help infer higher-order correlation functions [101], particle number fluctuations, and surface roughness [39,41,54,102–104] to comprehend fluctuating hydrodynamics. Additionally, it remains to be seen whether these methods exhibit robustness against dephasing and particle losses: in principle, PCA can be complemented with specific noise-filtering methods [100], a particularly attractive tool to mitigate the effect of dissipation effects. Another interesting perspective is to apply the methods discussed here to dynamical phenomena beyond transport, including quantum thermalization and ergodicity breaking, particularly to probe the concept of deep thermalization and complete Hilbert-space ergodicity [105–109], which have strong information-theoretic grounds. We leave these questions to future investigations.

The simulations were performed using the JULIA version of ITENSOR [110,111] and QUSPIN [112,113] libraries, respectively.

ACKNOWLEDGMENTS

We thank M. Heyl, Z. Lenarčič, M. Ljubotina, A. Scardicchio, M. Serbyn, C. Vanoni, and L. Vidmar for the discussions. We also thank R. S. Cortes, A. Gambassi, A. Jelic, R. K. Panda, and V. Vitale for collaboration on related projects, and the group of J. Barbier for discussions on principal component analysis theory. M.D. was partly supported by the ERC Consolidator grant Wavenets, by the QUANTERA DYNAMITE PCI2022-132919, by the EU-Flagship programme Pasquans2, by the PNRR MUR Project No. PE0000023-NQSTI, and by the PRIN programme (project CoQuS). M.A. received funding from the Deutsche Forschungsgemeinschaft (DFG, German Research Foundation) via Research Unit FOR5522 under Project No. 499180199 and under Germany's Excellence Strategy–EXC-2111–Grant No. 390814868. This publication has further received funding under Horizon Europe programme HORIZON-CL4- 2022-QUANTUM-02-SGA via the Project No. 101113690 (PASQuanS2.1).

[1] G. Carleo, I. Cirac, K. Cranmer, L. Daudet, M. Schuld, N. Tishby, L. Vogt-Maranto, and L. Zdeborová, Machine learning and the physical sciences, Rev. Mod. Phys. **91**, 045002 (2019).

[2] L. Wang, Discovering phase transitions with unsupervised learning, Phys. Rev. B **94**, 195105 (2016).

[3] W. Hu, R. R. P. Singh, and R. T. Scalettar, Discovering phases, phase transitions, and crossovers through unsupervised machine learning: A critical examination, Phys. Rev. E **95**, 062122 (2017).

[4] S. J. Wetzel, Unsupervised learning of phase transitions: From principal component analysis to variational autoencoders, Phys. Rev. E **96**, 022140 (2017).

[5] J. F. Rodriguez-Nieva and M. S. Scheurer, Identifying topological order through unsupervised machine learning, Nat. Phys. **15**, 790 (2019).

[6] A. Lidiak and Z. Gong, Unsupervised machine learning of quantum phase transitions using diffusion maps, Phys. Rev. Lett. **125**, 225701 (2020).

[7] T. Mendes-Santos, X. Turkeshi, M. Dalmonte, and A. Rodriguez, Unsupervised learning universal critical behavior via the intrinsic dimension, Phys. Rev. X **11**, 011040 (2021).

[8] A. Bohrdt, S. Kim, A. Lukin, M. Rispoli, R. Schittko, M. Knap, M. Greiner, and J. Léonard, Analyzing nonequilibrium quantum states through snapshots with artificial neural networks, Phys. Rev. Lett. **127**, 150504 (2021).

[9] J. Shen, W. Li, S. Deng, and T. Zhang, Supervised and unsupervised learning of directed percolation, Phys. Rev. E **103**, 052140 (2021).

[10] J. Shen, W. Li, S. Deng, D. Xu, S. Chen, and F. Liu, Machine learning of pair-contact process with diffusion, Sci. Rep. **12**, 19728 (2022).

[11] R. Verdel, V. Vitale, R. K. Panda, E. D. Donkor, A. Rodriguez, S. Lannig, Y. Deller, H. Strobel, M. K. Oberthaler, and M. Dalmonte, Data-driven discovery of statistically relevant information in quantum simulators, Phys. Rev. B **109**, 075152 (2024).

[12] Y. Tang, J. Liu, J. Zhang, and P. Zhang, Learning nonequilibrium statistical mechanics and dynamical phase transitions, Nat. Commun. **15**, 1117 (2024).

[13] C. Muzzi, R. S. Cortes, D. S. Bhakuni, A. Jelić, A. Gambassi, M. Dalmonte, and R. Verdel, Principal component analysis of absorbing state phase transitions, arXiv:2405.12863.

[14] J. Zang, M. Medvidović, D. Kiese, D. Di Sante, A. M. Sengupta, and A. J. Millis, Machine learning-based compression of quantum many body physics: PCA and autoencoder representation of the vertex function, arXiv:2403.15372.

[15] A. Polkovnikov, K. Sengupta, A. Silva, and M. Vengalattore, *Colloquium:* Nonequilibrium dynamics of closed interacting quantum systems, Rev. Mod. Phys. **83**, 863 (2011).

[16] R. Vasseur and J. E. Moore, Nonequilibrium quantum dynamics and transport: From integrability to many-body localization, J. Stat. Mech.: Theory Expt. (2016) 064010.

[17] J. Eisert, M. Friesdorf, and C. Gogolin, Quantum many-body systems out of equilibrium, Nat. Phys. **11**, 124 (2015).

[18] V. Khemani, A. Lazarides, R. Moessner, and S. L. Sondhi, Phase structure of driven quantum systems, Phys. Rev. Lett. **116**, 250401 (2016).

[19] D. V. Else, B. Bauer, and C. Nayak, Floquet time crystals, Phys. Rev. Lett. **117**, 090402 (2016).

[20] D. V. Else, C. Monroe, C. Nayak, and N. Y. Yao, Discrete time crystals, Annu. Rev. Condens. Matter Phys. **11**, 467 (2020).

[21] N. H. Lindner, G. Refael, and V. Galitski, Floquet topological insulator in semiconductor quantum wells, Nat. Phys. **7**, 490 (2011).

[22] F. Machado, D. V. Else, G. D. Kahanamoku-Meyer, C. Nayak, and N. Y. Yao, Long-range prethermal phases

of nonequilibrium matter, Phys. Rev. X **10**, 011043 (2020).
[23] M. S. Rudner, N. H. Lindner, E. Berg, and M. Levin, Anomalous edge states and the bulk-edge correspondence for periodically driven two-dimensional systems, Phys. Rev. X **3**, 031005 (2013).
[24] K. Wintersperger, C. Braun, F. N. Ünal, A. Eckardt, M. D. Liberto, N. Goldman, I. Bloch, and M. Aidelsburger, Realization of an anomalous Floquet topological system with ultracold atoms, Nat. Phys. **16**, 1058 (2020).
[25] M. Kardar, G. Parisi, and Y.-C. Zhang, Dynamic scaling of growing interfaces, Phys. Rev. Lett. **56**, 889 (1986).
[26] G. Müller, Anomalous spin diffusion in classical Heisenberg magnets, Phys. Rev. Lett. **60**, 2785 (1988).
[27] R. W. Gerling and D. P. Landau, Comment on anomalous spin diffusion in classical Heisenberg magnets, Phys. Rev. Lett. **63**, 812 (1989).
[28] R. W. Gerling and D. P. Landau, Time-dependent behavior of classical spin chains at infinite temperature, Phys. Rev. B **42**, 8214 (1990).
[29] K. Agarwal, S. Gopalakrishnan, M. Knap, M. Müller, and E. Demler, Anomalous diffusion and Griffiths effects near the many-body localization transition, Phys. Rev. Lett. **114**, 160401 (2015).
[30] Y. B. Lev, G. Cohen, and D. R. Reichman, Absence of diffusion in an interacting system of spinless fermions on a one-dimensional disordered lattice, Phys. Rev. Lett. **114**, 100601 (2015).
[31] Z. Cai, 1 / 3 Power-Law universality class out of stochastic driving in interacting systems, Phys. Rev. Lett. **128**, 050601 (2022).
[32] X. Cao, A. Tilloy, and A. De Luca, Entanglement in a fermion chain under continuous monitoring, SciPost Phys. **7**, 024 (2019).
[33] I. Corwin, Kardar-Parisi-Zhang universality, Notices Amer. Math. Soc. **63**, 230 (2016).
[34] H. Spohn, Nonlinear fluctuating hydrodynamics for anharmonic chains, J. Stat. Phys. **154**, 1191 (2014).
[35] A. Das, K. Damle, A. Dhar, D. A. Huse, M. Kulkarni, C. B. Mendl, and H. Spohn, Nonlinear fluctuating hydrodynamics for the classical XXZ spin chain, J. Stat. Phys. **180**, 238 (2020).
[36] M. Dupont and J. E. Moore, Universal spin dynamics in infinite-temperature one-dimensional quantum magnets, Phys. Rev. B **101**, 121106(R) (2020).
[37] Q. Fontaine, D. Squizzato, F. Baboux, I. Amelio, A. Lemaître, M. Morassi, I. Sagnes, L. Le Gratiet, A. Harouri, M. Wouters, I. Carusotto, A. Amo, M. Richard, A. Minguzzi, L. Canet, S. Ravets, and J. Bloch, Kardar–Parisi–Zhang universality in a one-dimensional polariton condensate, Nature (London) **608**, 687 (2022).
[38] B. Ye, F. Machado, J. Kemp, R. B. Hutson, and N. Y. Yao, Universal Kardar-Parisi-Zhang dynamics in integrable quantum systems, Phys. Rev. Lett. **129**, 230602 (2022).
[39] K. Fujimoto, R. Hamazaki, and Y. Kawaguchi, Family-Vicsek scaling of roughness growth in a strongly interacting Bose gas, Phys. Rev. Lett. **124**, 210604 (2020).
[40] O. A. Castro-Alvaredo, B. Doyon, and T. Yoshimura, Emergent hydrodynamics in integrable quantum systems out of equilibrium, Phys. Rev. X **6**, 041065 (2016).
[41] D. S. Bhakuni and Y. B. Lev, Dynamic scaling relation in quantum many-body systems, Phys. Rev. B **110**, 014203 (2024).
[42] D. Wei, A. Rubio-Abadal, B. Ye, F. Machado, J. Kemp, K. Srakaew, S. Hollerith, J. Rui, S. Gopalakrishnan, N. Y. Yao, I. Bloch, and J. Zeiher, Quantum gas microscopy of Kardar-Parisi-Zhang superdiffusion, Science **376**, 716 (2022).
[43] A. Scheie, N. E. Sherman, M. Dupont, S. E. Nagler, M. B. Stone, G. E. Granroth, J. E. Moore, and D. A. Tennant, Detection of Kardar-Parisi-Zhang hydrodynamics in a quantum Heisenberg spin-1/2 chain, Nat. Phys. **17**, 726 (2021).
[44] P. N. Jepsen, J. Amato-Grill, I. Dimitrova, W. W. Ho, E. Demler, and W. Ketterle, Spin transport in a tunable Heisenberg model realized with ultracold atoms, Nature (London) **588**, 403 (2020).
[45] N. Keenan, N. F. Robertson, T. Murphy, S. Zhuk, and J. Goold, Evidence of Kardar-Parisi-Zhang scaling on a digital quantum simulator, npj Quantum Inf. **9**, 72 (2023).
[46] M. Hopjan and L. Vidmar, Scale-invariant critical dynamics at eigenstate transitions, Phys. Rev. Res. **5**, 043301 (2023).
[47] M. Hopjan and L. Vidmar, Scale-invariant survival probability at eigenstate transitions, Phys. Rev. Lett. **131**, 060404 (2023).
[48] A. J. McRoberts, T. Bilitewski, M. Haque, and R. Moessner, Anomalous dynamics and equilibration in the classical Heisenberg chain, Phys. Rev. B **105**, L100403 (2022).
[49] A. J. McRoberts, T. Bilitewski, M. Haque, and R. Moessner, Long-lived solitons and their signatures in the classical Heisenberg chain, Phys. Rev. E **106**, L062202 (2022).
[50] C. Gross and W. S. Bakr, Quantum gas microscopy for single atom and spin detection, Nat. Phys. **17**, 1316 (2021).
[51] A. Impertro, S. Karch, J. F. Wienand, S. Huh, C. Schweizer, I. Bloch, and M. Aidelsburger, Local readout and control of current and kinetic energy operators in optical lattices, Phys. Rev. Lett. **133**, 063401 (2024).
[52] H. Bernien, S. Schwartz, A. Keesling, H. Levine, A. Omran, H. Pichler, S. Choi, A. S. Zibrov, M. Endres, M. Greiner, V. Vuletić, and M. D. Lukin, Probing many-body dynamics on a 51-atom quantum simulator, Nature (London) **551**, 579 (2017).
[53] M. K. Joshi, F. Kranzl, A. Schuckert, I. Lovas, C. Maier, R. Blatt, M. Knap, and C. F. Roos, Observing emergent hydrodynamics in a long-range quantum magnet, Science **376**, 720 (2022).
[54] J. F. Wienand, S. Karch, A. Impertro, C. Schweizer, E. McCulloch, R. Vasseur, S. Gopalakrishnan, M. Aidelsburger, and I. Bloch, Emergence of fluctuating hydrodynamics in chaotic quantum systems, Nat. Phys. (2024), doi:10.1038/s41567-024-02611-z.
[55] A. Browaeys and T. Lahaye, Many-body physics with individually controlled Rydberg atoms, Nat. Phys. **16**, 132 (2020).
[56] I. T. Jolliffe and J. Cadima, Principal component analysis: A review and recent developments, Phil. Trans. R. Soc. A. **374**, 20150202 (2016).
[57] X. Zotos, Finite temperature drude weight of the one-dimensional spin- 1/2 Heisenberg model, Phys. Rev. Lett. **82**, 1764 (1999).
[58] M. Žnidarič, Spin transport in a one-dimensional anisotropic Heisenberg model, Phys. Rev. Lett. **106**, 220601 (2011).

[59] M. Ljubotina, M. Žnidarič, and T. Prosen, Spin diffusion from an inhomogeneous quench in an integrable system, Nat. Commun. **8**, 16117 (2017).
[60] M. Ljubotina, M. Žnidarič, and T. Prosen, Kardar-Parisi-Zhang physics in the quantum Heisenberg magnet, Phys. Rev. Lett. **122**, 210602 (2019).
[61] S. Gopalakrishnan and R. Vasseur, Kinetic theory of spin diffusion and superdiffusion in XXZ spin chains, Phys. Rev. Lett. **122**, 127202 (2019).
[62] V. B. Bulchandani, R. Vasseur, C. Karrasch, and J. E. Moore, Bethe-Boltzmann hydrodynamics and spin transport in the XXZ chain, Phys. Rev. B **97**, 045407 (2018).
[63] J. De Nardis, D. Bernard, and B. Doyon, Hydrodynamic diffusion in integrable systems, Phys. Rev. Lett. **121**, 160603 (2018).
[64] M. Dupont, N. E. Sherman, and J. E. Moore, Spatiotemporal crossover between low- and high-temperature dynamical regimes in the quantum Heisenberg magnet, Phys. Rev. Lett. **127**, 107201 (2021).
[65] J. De Nardis, S. Gopalakrishnan, E. Ilievski, and R. Vasseur, Superdiffusion from emergent classical solitons in quantum spin chains, Phys. Rev. Lett. **125**, 070601 (2020).
[66] J. De Nardis, M. Medenjak, C. Karrasch, and E. Ilievski, Anomalous spin diffusion in one-dimensional antiferromagnets, Phys. Rev. Lett. **123**, 186601 (2019).
[67] E. Ilievski, J. De Nardis, M. Medenjak, and T. Prosen, Superdiffusion in one-dimensional quantum lattice models, Phys. Rev. Lett. **121**, 230602 (2018).
[68] J. De Nardis, S. Gopalakrishnan, and R. Vasseur, Nonlinear fluctuating hydrodynamics for Kardar-Parisi-Zhang scaling in isotropic spin chains, Phys. Rev. Lett. **131**, 197102 (2023).
[69] E. Ilievski, J. De Nardis, S. Gopalakrishnan, R. Vasseur, and B. Ware, Superuniversality of superdiffusion, Phys. Rev. X **11**, 031023 (2021).
[70] S. Gopalakrishnan, A. Morningstar, R. Vasseur, and V. Khemani, Distinct universality classes of diffusive transport from full counting statistics, Phys. Rev. B **109**, 024417 (2024).
[71] Ž. Krajnik, E. Ilievski, and T. Prosen, Absence of normal fluctuations in an integrable magnet, Phys. Rev. Lett. **128**, 090604 (2022).
[72] Ž. Krajnik, J. Schmidt, E. Ilievski, and T. Prosen, Dynamical criticality of magnetization transfer in integrable spin chains, Phys. Rev. Lett. **132**, 017101 (2024).
[73] M. Ljubotina, L. Zadnik, and T. Prosen, Ballistic spin transport in a periodically driven integrable quantum system, Phys. Rev. Lett. **122**, 150605 (2019).
[74] V. B. Bulchandani, S. Gopalakrishnan, and E. Ilievski, Superdiffusion in spin chains, J. Stat. Mech.: Theory Expt. (2021) 084001.
[75] S. Nandy, Z. Lenarčič, E. Ilievski, M. Mierzejewski, J. Herbrych, and P. Prelovšek, Spin diffusion in a perturbed isotropic Heisenberg spin chain, Phys. Rev. B **108**, L081115 (2023).
[76] E. Rosenberg, T. I. Andersen, R. Samajdar, A. Petukhov, J. C. Hoke, D. Abanin, A. Bengtsson, I. K. Drozdov, C. Erickson, P. V. Klimov, X. Mi, A. Morvan, M. Neeley, C. Neill, R. Acharya, R. Allen, K. Anderson, M. Ansmann, F. Arute, K. Arya *et al.*, Dynamics of magnetization at infinite temperature in a Heisenberg spin chain, Science **384**, 48 (2024).
[77] P. N. Jepsen, W. W. Ho, J. Amato-Grill, I. Dimitrova, E. Demler, and W. Ketterle, Transverse spin dynamics in the anisotropic Heisenberg model realized with ultracold atoms, Phys. Rev. X **11**, 041054 (2021).
[78] S. Hild, T. Fukuhara, P. Schauß, J. Zeiher, M. Knap, E. Demler, I. Bloch, and C. Gross, Far-from-equilibrium spin transport in Heisenberg quantum magnets, Phys. Rev. Lett. **113**, 147205 (2014).
[79] P. Peng, B. Ye, N. Y. Yao, and P. Cappellaro, Exploiting disorder to probe spin and energy hydrodynamics, Nat. Phys. **19**, 1027 (2023).
[80] Y.-H. Shi, Z.-H. Sun, Y.-Y. Wang, Z.-A. Wang, Y.-R. Zhang, W.-G. Ma, H.-T. Liu, K. Zhao, J.-C. Song, G.-H. Liang, Z.-Y. Mei, J.-C. Zhang, H. Li, C.-T. Chen, X. Song, J. Wang, G. Xue, H. Yu, K. Huang, Z. Xiang *et al.*, Probing spin hydrodynamics on a superconducting quantum simulator, Nat. Commun. **15**, 7573 (2024).
[81] Y. Li, T.-G. Zhou, Z. Wu, P. Peng, S. Zhang, R. Fu, R. Zhang, W. Zheng, P. Zhang, H. Zhai *et al.*, Emergent universal quench dynamics in randomly interacting spin models, Nat. Phys. (2024), doi:10.1038/s41567-024-02664-0.
[82] H. Kim and D. A. Huse, Ballistic spreading of entanglement in a diffusive nonintegrable system, Phys. Rev. Lett. **111**, 127205 (2013).
[83] M. Schulz, S. R. Taylor, C. A. Hooley, and A. Scardicchio, Energy transport in a disordered spin chain with broken U (1) symmetry: Diffusion, subdiffusion, and many-body localization, Phys. Rev. B **98**, 180201(R) (2018).
[84] M. Ljubotina, J.-Y. Desaules, M. Serbyn, and Z. Papić, Superdiffusive energy transport in kinetically constrained models, Phys. Rev. X **13**, 011033 (2023).
[85] V. K. Varma, A. Lerose, F. Pietracaprina, J. Goold, and A. Scardicchio, Energy diffusion in the ergodic phase of a many body localizable spin chain, J. Stat. Mech.: Theory Expt. (2017) 053101.
[86] We note that the analysis can be immediately extended in the case of other types of evolution (e.g., Floquet or open quantum systems such as boundary driven chains).
[87] In classical simulations, wave function snapshots can be sampled, for instance, via perfect sampling [96] in matrix-product-state-based computations.
[88] R. K. Panda, R. Verdel, A. Rodriguez, H. Sun, G. Bianconi, and M. Dalmonte, Non-parametric learning critical behavior in Ising partition functions: PCA entropy and intrinsic dimension, SciPost Phys. Core **6**, 086 (2023).
[89] C. Vanoni and V. Vitale, Analysis of localization transitions using nonparametric unsupervised learning, Phys. Rev. B **110**, 024204 (2024).
[90] M. Žnidarič, A. Scardicchio, and V. K. Varma, Diffusive and subdiffusive spin transport in the ergodic phase of a many-body localizable system, Phys. Rev. Lett. **117**, 040601 (2016).
[91] G. Misguich, K. Mallick, and P. L. Krapivsky, Dynamics of the spin-$\frac{1}{2}$ Heisenberg chain initialized in a domain-wall state, Phys. Rev. B **96**, 195151 (2017).
[92] B. Ye, F. Machado, C. D. White, R. S. K. Mong, and N. Y. Yao, Emergent hydrodynamics in nonequilibrium quantum systems, Phys. Rev. Lett. **125**, 030601 (2020).
[93] G. Vidal, Efficient classical simulation of slightly entangled quantum computations, Phys. Rev. Lett. **91**, 147902 (2003).

[94] G. Vidal, Efficient simulation of one-dimensional quantum many-body systems, Phys. Rev. Lett. **93**, 040502 (2004).
[95] E. Stoudenmire and S. R. White, Minimally entangled typical thermal state algorithms, New J. Phys. **12**, 055026 (2010).
[96] A. J. Ferris and G. Vidal, Perfect sampling with unitary tensor networks, Phys. Rev. B **85**, 165146 (2012).
[97] A. Blum, J. Hopcroft, and R. Kannan, *Foundations of Data Science* (Cambridge University Press, Cambridge, 2020).
[98] Alternatively, a more experimentally feasible option involves a product state wherein one-half of the system is fully polarized in the z direction, while the other half is prepared in a Néel state.
[99] P. Fendley, K. Sengupta, and S. Sachdev, Competing density-wave orders in a one-dimensional hard-boson model, Phys. Rev. B **69**, 075106 (2004).
[100] J. Barbier, F. Camilli, M. Mondelli, and M. Sáenz, Fundamental limits in structured principal component analysis and how to reach them, Proc. Natl. Acad. Sci. USA **120**, e2302028120 (2023).
[101] M. Rispoli, A. Lukin, R. Schittko, S. Kim, M. E. Tai, J. Léonard, and M. Greiner, Quantum critical behaviour at the many-body localization transition, Nature (London) **573**, 385 (2019).
[102] K. Fujimoto, R. Hamazaki, and Y. Kawaguchi, Dynamical scaling of surface roughness and entanglement entropy in disordered Fermion models, Phys. Rev. Lett. **127**, 090601 (2021).
[103] K. Fujimoto and T. Sasamoto, Exact solution of bipartite fluctuations in one-dimensional fermions, arXiv:2403.18523.
[104] S. Aditya and N. Roy, Family-Vicsek dynamical scaling and Kardar-Parisi-Zhang-like superdiffusive growth of surface roughness in a driven one-dimensional quasiperiodic model, Phys. Rev. B **109**, 035164 (2024).
[105] J. Choi, A. L. Shaw, I. S. Madjarov, X. Xie, R. Finkelstein, J. P. Covey, J. S. Cotler, D. K. Mark, H.-Y. Huang, A. Kale, H. Pichler, F. G. S. L. Brandão, S. Choi, and M. Endres, Preparing random states and benchmarking with many-body quantum chaos, Nature (London) **613**, 468 (2023).
[106] J. S. Cotler, D. K. Mark, H.-Y. Huang, F. Hernández, J. Choi, A. L. Shaw, M. Endres, and S. Choi, Emergent quantum state designs from individual many-body wave functions, PRX Quantum **4**, 010311 (2023).
[107] S. Pilatowsky-Cameo, C. B. Dag, W. W. Ho, and S. Choi, Complete Hilbert-space ergodicity in quantum dynamics of generalized Fibonacci drives, Phys. Rev. Lett. **131**, 250401 (2023).
[108] D. K. Mark, F. Surace, A. Elben, A. L. Shaw, J. Choi, G. Refael, M. Endres, and S. Choi, A maximum entropy principle in deep thermalization and in Hilbert-space ergodicity, arXiv:2403.11970.
[109] A. L. Shaw, D. K. Mark, J. Choi, R. Finkelstein, P. Scholl, S. Choi, and M. Endres, Universal fluctuations and noise learning from Hilbert-space ergodicity, arXiv:2403.11971.
[110] M. Fishman, S. R. White, and E. M. Stoudenmire, The ITensor software library for tensor network calculations, SciPost Phys. Codebases, 4 (2022).
[111] M. Fishman, S. R. White, and E. M. Stoudenmire, Codebase release 0.3 for ITensor, SciPost Phys. Codebases, 4 (2022).
[112] P. Weinberg and M. Bukov, QuSpin: a PYTHON package for dynamics and exact diagonalisation of quantum many body systems, Part I: Spin chains, SciPost Phys. **2**, 003 (2017).
[113] P. Weinberg and M. Bukov, QuSpin: a PYTHON package for dynamics and exact diagonalisation of quantum many body systems. Part II: Bosons, fermions and higher spins, SciPost Phys. **7**, 020 (2019).